VALVE POSITION TRACKING FOR SOFT LANDING OF ELECTROMECHANICAL CAMLESS VALVETRAIN

Wolfgang Hoffmann * **Anna G. Stefanopoulou** **

* *Siemens AG, Frauenauracherstr.80, 91056 Erlangen, Germany*
** *Mechanical Engineering, University of Michigan, G058 WE Lay Auto Lab, 1231 Beal Ave, Ann Arbor MI 48109-2121, USA*

Abstract: Variable valve opening and closing allows improvements of internal combustion engines and requires precise control of the camless valvetrain actuator. In this paper the valve position tracking in electromechanical camless valvetrains (EMCV) is considered. One of the main problems in the EMCV actuator is the noise and wear associated with high contact velocities during the closing and opening of the valve. The contact velocity of the actuator and the valve can be reduced, and thus, noise and wear, by designing a tracking controller that consists of a linear feedback and an iterative learning controller (ILC). With the ILC methodology every cycle the feedforward signal of the feedback controller is updated based on the error between the actual valve position and the desired position. The methodology is reviewed and simulation results are presented. *Copyright ©2001 IFAC*

Keywords: learning control, valve, automotive, electromagnetic, singular value decomposition

1. INTRODUCTION

Various studies have shown that optimization of the valve timing of an automotive internal combustion engine results in high fuel efficiency, low emissions and improved torque performance. Because of the potential benefits many automotive engine manufacturers and research laboratories are developing mechanisms that can provide the valve event variability. A promising mechanism is the electromechanical camless valvetrain actuator. It relies on two electromagnets that catch and hold an armature that moves with a damped oscillation between two extreme positions under the forcing of two springs. The control signal to the electromechanical actuator is the voltage applied to the coils of the two electromagnets. The control objective is to ensure accurate valve opening and closing with small contact velocity of all the moving parts. The small contact velocity, also known as "soft landing," is a very important consideration because high contact velocities correlate with noise and increased component wear. Soft landing is difficult to achieve under real operating conditions (Butzmann *et al.* 2000) due to (i) varying reference trajectories depending on various engine speeds and loads, and (ii) unknown gas forces acting on the valves.

To address the problem a tracking controller for the valve position $Y(t)$ is designed. The desired valve opening and closing reference trajectory $Y_d(t)$ is generated by the engine management system. The closed loop system comprises of a feedforward and a feedback controller. In particular, the feedback controller is a linear stabilizing controller that drives the armature to a desired constant position. It is designed based on linearization and discretization of the plant at an equilibrium point close to the contact point. It is important here to note that the plant is unstable at any equilibrium close to the contact point.

Furthermore, the discretization results in a non–minimum phase open loop system. In order to improve the transient behavior of the feedback controller, a feedforward controller is designed that calculates the desired armature position used by the feedback controller. This signal is updated between consecutive cycles (full armature travel) based on the error between the desired position $Y_d(t)$ and the actual position $Y(t)$ by using an Iterative Learning Control (ILC) methodology (Arimoto *et al.* 1984) and (Xu and Bien 1998).

The paper is organized as follows. Nomenclature is shown in tables in Sections 2. The electromechanical valve actuator model is briefly presented in Section 3. Analysis of the open loop system properties at different equilibrium points and linearization are discussed in Section 4. The controller structure and the closed loop system objectives are presented in Section 5. The linear feedback controller design and simulations are shown in Section 6. Section 7 shows the development of the learning controller. Closed loop simulations and some concluding remarks are presented in Section 8.

2. NOMENCLATURE

Table 1. Signals and parameters

Symbol	Unit	Explanation
(Y_d), Y	m	(desired) armature position
V	$\frac{m}{s}$	armature velocity
$U_{u/l}$	V	voltage upper / lower coil
$I_{u/l}$	A	current upper / lower coil
$\Phi_{u/l}$	$\frac{Nm}{A}$	flux upper / lower coil
$F_{u/l}$	N	magnetic force
F_{flow}	N	force due to gas airflow
m	kg	mass of moving part
G	$\frac{kg}{s}$	friction coef
D	$\frac{kg}{s^2}$	spring constant
$2h$	m	thickness of disc
R	Ω	el. resistance of a coil

Table 2. Notation

$S(t)$	continous time signal
$S[n]$	discrete time signal
S^0	signal at equilibrium point (e.p.)
$s[n] = S[n] - S^0$	deviation between signal and e.p.
$s[n,k]$	discrete signal of the k^{th} cycle
$\boldsymbol{v}$	vector
$\boldsymbol{M}$	matrix

3. MODEL

A brief description of the model of the EMVC actuator is presented. For detailed analysis and validation of the model see (Wang *et al.* 2000).

A model of the actuator consists of a mechanical, electrical and a magnetic subsystem. For an explanation of symbols and parameters see tables 1 and 2. The mechanical subsystem can be modelled as a spring–mass–damper system including the external magnetic forces F_u of the upper and F_l of the lower electromagnet. A force balance yields

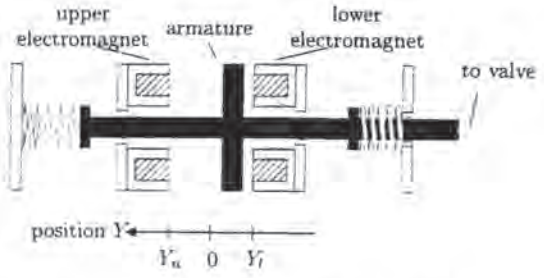

Fig. 1. Electromagnetic actuator of the valve

$$m\frac{\mathrm{d}V(t)}{\mathrm{d}t} = -DY(t) - GV(t) + F_l(t) + F_u(t) \quad (1)$$

The two coils are modelled by an electrical subsystem, consisting of a resistance/reluctance–circuit. The coil reluctances are inversely proportional to the armature gaps $Y - Y_l - h$ or $Y_u - Y - h$, respectively. The coil currents $I_{l/u}(t)$ are modeled with a nonlinear function f_I of the armature gap and the flux, yielding

$$U_l(t) = R\,\mathrm{f}_I(\Phi_l, Y - Y_l - h) + \frac{\mathrm{d}\Phi_l(t)}{\mathrm{d}t} \quad (2)$$

and

$$U_u(t) = R\,\mathrm{f}_I(\Phi_u, Y_u - Y - h) + \frac{\mathrm{d}\Phi_u(t)}{\mathrm{d}t} \quad (3)$$

as the two equations for the lower and upper coil, respectively. The mechanical and electrical subsystems are linked by the magnetic force equations of the two electromagnets,

$$F_l = -\mathrm{f}_{mag}(\Phi_l, Y - Y_l - h)$$

and

$$F_u = \mathrm{f}_{mag}(\Phi_u, Y_u - Y - h).$$

Their form is given by

$$\mathrm{f}_I(\Phi, Y) = \frac{\Phi}{L_f - \Delta L_f\left(1 - e^{-\frac{Y}{Y_f}}\right)}$$

and

$$\mathrm{f}_{mag}(\Phi, Y) = \frac{\Delta L_f \Phi^2 e^{-\frac{Y}{Y_f}}}{2Y_f\left(L_f - \Delta L_f\left[1 - e^{-\frac{Y}{Y_f}}\right]\right)^2}.$$

To sumarize, the plant has two inputs, upper voltage $U_u(t)$ and lower voltage $U_l(t)$, respectively. The plant output is the armature position $Y(t)$. The four elements of the state vector are position $Y(t)$, velocity $V(t)$, lower flux $\Phi_l(t)$ and the upper flux $\Phi_u(t)$.

Thus, the state-space description of the model is given by

$$\frac{\mathrm{d}Y}{\mathrm{d}t} = V \tag{4}$$

$$\frac{\mathrm{d}V}{\mathrm{d}t} = -\frac{D}{m}Y - \frac{G}{m}V + \frac{F_u}{m} + \frac{F_l}{m} \tag{5}$$

$$\frac{\mathrm{d}\Phi_u}{\mathrm{d}t} = -R\mathrm{f}_I\left(\Phi_u, Y_u - Y - h\right) + U_u \tag{6}$$

$$\frac{\mathrm{d}\Phi_l}{\mathrm{d}t} = -R\mathrm{f}_I\left(\Phi_l, Y - Y_l - h\right) + U_l. \tag{7}$$

A block diagram representation of above equations is shown in figure 4. The upper coil is not included because of symmetry. The model is implemented in Matlab/Simulink.

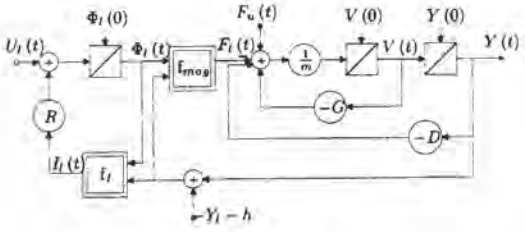

Fig. 2. Blockdiagram of the EMV actuator model without representation of the upper coil.

4. ANALYSIS

4.1 *Equilibria*

In order to obtain equilibrium points of the model, the state space equations have to be solved for $\frac{d}{dt}\left[Y(t), V(t), \Phi_l(t), \Phi_u(t)\right] \equiv \mathbf{0}$ and constant inputs. The assumption $U_u(t) \equiv 0$ and $U_l(t) \equiv U_l^0$ yields a stable equilibrium point at $\left[0, 0, \Phi_l^0, 0\right]^T$ and an unstable e.p. at $\left[Y^0, 0, \Phi_l^0, 0\right]^T$. Figure 3 shows U_l^0 versus Y^0. As the figure shows, the system cannot be driven into the unstable equilibrium point if $Y^0 \geq -3.25mm$ due to voltage saturation at $U_l^{max} = 200V$.

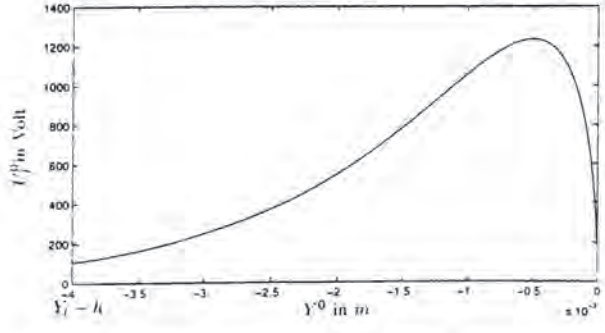

Fig. 3. Voltage in the unstable equilibrium points for various positions. Dotted line: Maimum Voltage of the available source. For $Y^0 = Y_l - h$, the gap is closed.

4.2 *Linearization and Discretization*

The analysis of the plant is continued by linearizing the state–space equations around one of the above examined unstable equilibrium points. The magnetic force of the upper coil F_u is approximately zero in equilibrium points $Y^0 \leq -3.5mm$. Thus the input $U_u(t)$ and equation 6 don't have to be considered in the following linearization. The state vector reduces to $\left[Y(t), V(t), \Phi_l(t)\right]^T$. A linear state–space description

$$\frac{\mathrm{d}\boldsymbol{x}}{\mathrm{d}t} = \boldsymbol{A}_0\boldsymbol{x} + \boldsymbol{b}_0 u_l \tag{8}$$

$$y = \boldsymbol{c}_0{}^T\boldsymbol{x}. \tag{9}$$

can be derived by linearization of the model equations. $\boldsymbol{x} = \left[y(t), v(t), \varphi_l(t)\right]^T$ is the deviation of the states from the nominal equilibrium point $\left[Y^0, V^0, \Phi^0\right]$ (Table 2).

In the next section, a discrete controller for the plant is designed, as in practise the plant output $Y(t)$ will be sampled and the input $U_l(t)$ will be the result of a zero order hold operation. The three poles and two zeros of the corresponding discrete transfer–function depend on the equilibrium point. Their locations in the z-plane are shown in figure 4. The linearized and discretized plant is unstable and non–minimum phase in all the considered equilibrium points.

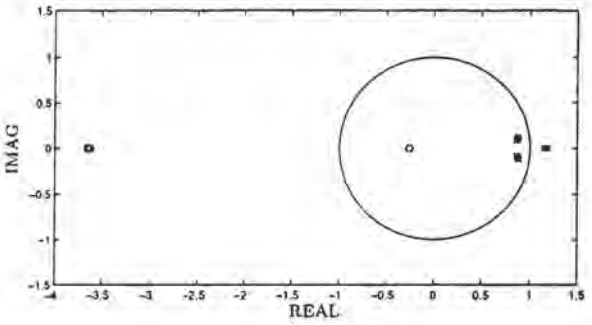

Fig. 4. Zeros and poles loci of the linearized discrete plant in the equilibrium points $(Y^0 - Y_l - h) \in [0, 1, 2, 3, 4, 5] \cdot 0.1mm$. The sample time is choosen to be $T_S = 0.1ms$.

5. CONTROLLER STRUCTURE

The EMCV control system is required to:

- Ensure accurate valve closing and opening events (timing). Variable valve timing is used to optimize the engine operation with respect to emissions, fuel economy, and drivability. The engine management system typically generates these commands based on the driver's torque demand and other vehicle variables.

- Reduce the armature-coil and valve-cylinder contact velocities. High contact velocity results in noise and component wear. Engine manufacturers are designing camshafts to achieve a low 0.04 m/sec contact velocity at low engine speeds. The contact velocity in conventionally driven valves increases linearly with engine speed.

To achieve the above two requirements that are sometimes conflicting a controller that achieves tracking of a reference trajectory $Y_d[n]$ with the desired timing and contact velocity is designed.

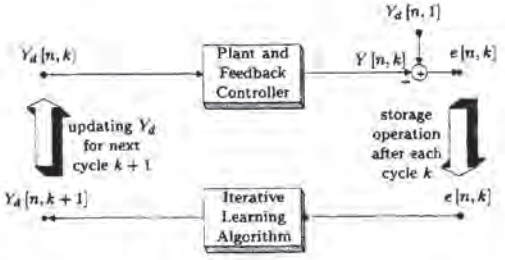

Fig. 5. The controller structure. An Iterative Learning Controller is applied to a closed loop system consisting of the plant and an observer based feedback controller.

Figure 5 shows the controller structure. The block "Plant and feedback controller" consists of an observer based feedback controller used to stabilize the plant at an equilibrium point close to the contact point. In order to improve the transient behavior of the feedback controller, a feedforward controller changes the input of the closed loop system $Y_d[n]$. The new input is calculated by an Iterative Learning Controller (ILC), updating Y_d between consecutive cycles (full armature travel) k and $k+1$. The ILC is processing the error between the desired position $Y_d[n,1]$ and the actual position $Y[n,k]$. Detailed information about the learning controller is given in section 7. The next section discusses the design of the feedback controller.

6. DESIGN OF THE FEEDBACK CONTROLLER

The armature is assumed to be held by the upper electromagnet in the position $Y_u - h$ and then to be released by disconnecting the upper voltage source at $t = t_0$. As the armature approaches a defined position Y^{fb}, the plant input signal $U_l(t)$ is switched from a constant previous value U^{pre} to the feedback controller signal. Y^{fb} is a position not far from the feasible equilibrium points in figure 3. U^{pre} is used to preset the state $\Phi_l(t)$ close to the equilibrium point value Φ^0.

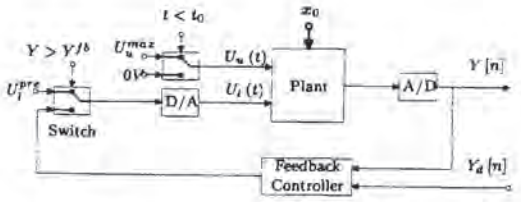

Fig. 6. Feedback controller structure.

As feedback controller, a linear-quadratic state-feedback regulator with observer is used, designed based on a linearization of the plant at $Y^0 = Y_l + h$. The state-feedback gain is choosen to minimize the cost functional

$$J = \int_0^\infty \boldsymbol{x}^T \boldsymbol{Q} \boldsymbol{x} + r u_l^2 dt.$$

A good compromise between fast control action and input saturation is the choice $\boldsymbol{Q} = I$ and $r = 1$. The observer poles are set four times faster than the resulting poles of the closed loop system. The controller input is never disconnected from the plant in order to reduce observer error. Finally, a discrete version of the controller is obtained by emulating the resulting controller functions using Tustin's method.

In figure 7 the dashed line shows the armature travel for the open loop system (damped oszillation). The solid line corresponds to the armature travel with the observer based feedback controller. Figure 8 shows a detail of the armature travel just before the contact with the lower coil, and 9 shows a comparison between the observed and the actual states.

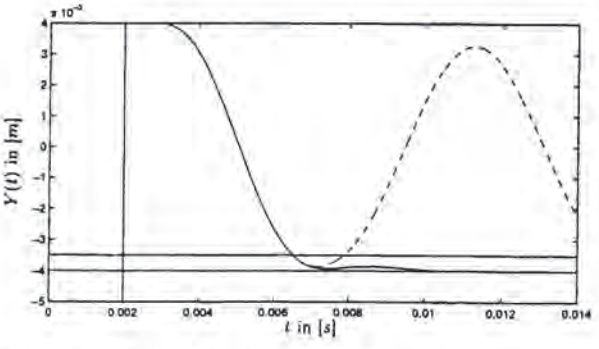

Fig. 7. Position of the armature with (solid) and without (dashed) feedback controler.

7. TRACKING USING ITERATIVE LEARNING CONTROL

In order to achieve better tracking of the desired position, the cyclic character of the process is exploited by use of the Iterative Learning Controller (ILC) introduced in section 5. The next paragraph explains ILC in brief, followed by a paragraph

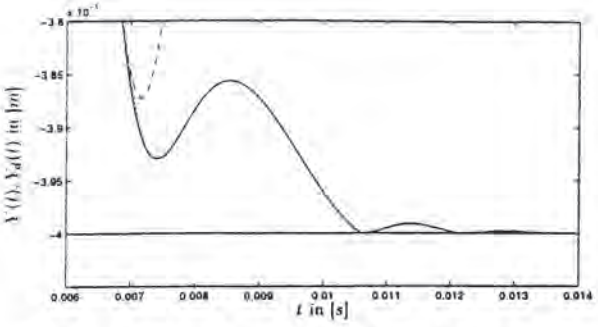

Fig. 8. A detailed version of figure 7. The controller is stabilizing, but the desired position Y_d (dotted) and position Y (solid) are not matching.

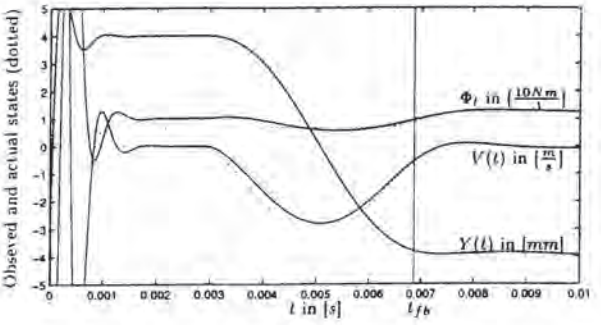

Fig. 9. Observed states (solid) tend to the states (dotted). Transient errors are small at t_{fb}, when the controller is switched on.

dedicated to the specific learning algorithm used in this paper.

7.1 *Iterative Learning Control*

The input and output sequences of the *closed loop* system are $Y_d[n]$ and $Y[n]$, respectively. To formulate ILC in a compact way, it makes sense to describe this mapping by defining the operator $\Gamma : \mathbf{R}^N \mapsto \mathbf{R}^N$ as $\boldsymbol{y} = \Gamma(\boldsymbol{y}_d)$, introducing the vectors

$$\boldsymbol{y}_d = \begin{bmatrix} y_d[n_{fb}] \\ \vdots \\ y_d[n_{fb}+N-1] \end{bmatrix}$$

and

$$\boldsymbol{y} = \begin{bmatrix} y[n_{fb}+1] \\ \vdots \\ y[n_{fb}+N] \end{bmatrix}.$$

n_{fb} is defined as the indice of the first sample after switching on the feedback controller. N is the number of values later involved in the ILC. As mentioned above, the lower case notation of a signal stands for its deviation from the equilibrium point.

The purpose of the ILC is to find some vector $\boldsymbol{y}_d^\star$ with the property $\boldsymbol{y}_d \cong \Gamma(\boldsymbol{y}_d^\star)$. In order to solve this problem, the cyclic opening and closing of the valve is exploited. Let the cycles be numbered with k. In the first cycle, the input vector $\boldsymbol{y}_d[1] \equiv \boldsymbol{y}_d$ is applied to the system. This vector and the corresponding output vector $\boldsymbol{y}[1]$ are used to generate an improved input vector $\boldsymbol{y}_d[2]$ for the next cycle, and so forth. Thus, a linear formulation of the ILC algorithm reads as

$$\boldsymbol{y}_d[k+1] = \boldsymbol{S}\boldsymbol{y}_d[k] + \boldsymbol{E}(\boldsymbol{y}_d[1] - \boldsymbol{y}[k]), \quad (10)$$

where the matrices $\boldsymbol{S}$ and $\boldsymbol{E}$ weight the previous input $\boldsymbol{y}_d[k]$ and the previous error $\boldsymbol{e}[k] = \boldsymbol{y}_d[1] - \boldsymbol{y}[k]$, respectively. They have to be choosen in a way that the sequence $\{\boldsymbol{y}_d[k]\}$ converges in the sense of the L_2-norm to

$$\boldsymbol{y}_d^\star = \lim_{k\to\infty} \boldsymbol{y}_d[k]. \quad (11)$$

7.2 *Design of the Learning Controller*

Similar to the the feedback controller, the learning controller is designed using the linearized model of the plant calculated in section 4.2. Define the convolution-matrix

$$\boldsymbol{P} = \begin{bmatrix} h[1] & 0 & 0 & \cdots & 0 \\ h[2] & h[1] & 0 & \cdots & 0 \\ \vdots & \vdots & & & \vdots \\ h[N-1] & h[N-2] & \cdots & h[1] & 0 \\ h[N] & h[N-1] & \cdots & h[2] & h[1] \end{bmatrix} \quad (12)$$

The matrix entries are the elements of the impulse response sequence $\{h[n]\}$ of the linearized, discretized closed loop system, therefore $\Gamma(\boldsymbol{y}_d) \cong \boldsymbol{P}\boldsymbol{y}_d$ holds true close to the equilibrium point.

To derive the learning controller used in this paper, the singular value decomposition (svd) is applied to the convolution-matrix

$$\boldsymbol{P} = \boldsymbol{L}\boldsymbol{\Lambda}\boldsymbol{R}^T, \quad (13)$$

where $\boldsymbol{R}$ and $\boldsymbol{L}$ are orthonormal matrices, $\boldsymbol{\Lambda}$ is a diagonal matrix with the elements $\sigma_0 > \sigma_i > 0 \;\; \forall \;\; i \in [1, N-1]$. The largest singular value σ_0 is the L_2-norm of $\boldsymbol{P}$. The learning algorithm is determined by setting

$$\boldsymbol{S} = \boldsymbol{I} \quad (14)$$

and

$$\boldsymbol{E} = \frac{1}{\sigma_0}\boldsymbol{R}\boldsymbol{L}^T. \quad (15)$$

This learning algorithm is now analyzed with the help of the discrete, linearized model. Using in equation 10 the linear model equation $\boldsymbol{y} = \boldsymbol{P}\boldsymbol{y}_d$ instead of $\boldsymbol{y} = \Gamma(\boldsymbol{y}_d)$ yields

$$\boldsymbol{y}_d[k+1] = \boldsymbol{S}\boldsymbol{y}_d[k] + \boldsymbol{E}\left(\boldsymbol{y}_d[1] - \boldsymbol{P}\boldsymbol{y}_d[k]\right) \quad (16)$$

With (13), (14) and (15) equation (16) can be written in the form

$$\boldsymbol{R}^T\boldsymbol{y}_d[k+1] = \left(\boldsymbol{I} - \frac{1}{\sigma_0}\boldsymbol{\Lambda}\right)\boldsymbol{R}^T\boldsymbol{y}_d[k] + \frac{1}{\sigma_0}\boldsymbol{L}^T\boldsymbol{y}_d[1]. \quad (17)$$

Involving the transformed vectors $\boldsymbol{\nu}[k] = \boldsymbol{R}^T\boldsymbol{y}_d[k]$ and $\boldsymbol{\mu} = \boldsymbol{L}^T\boldsymbol{y}_d[1]$, equation 17 reads as

$$\boldsymbol{\nu}[k+1] = \left(\boldsymbol{I} - \frac{1}{\sigma_0}\boldsymbol{\Lambda}\right)\boldsymbol{\nu}[k] + \frac{1}{\sigma_0}\boldsymbol{\mu}. \quad (18)$$

or rewritten in N separate equations

$$\nu_i[k+1] = \left(1 - \frac{\sigma_i}{\sigma_0}\right)\nu_i[k] + \frac{1}{\sigma_0}\mu_i \quad \forall \quad i \in [0, N-1]. \quad (19)$$

The above choice of $\boldsymbol{E}$ and $\boldsymbol{S}$ yields a decoupled learning algorithm. Thus, to determine the convergence of the learning controller the convergence properties of N scalar equations can be studied instead of a matrix equation. Solving the recursive equations (19) yields

$$\nu_i[k] = (1-\bar{\sigma}_i)^k\nu_i[0] + \frac{1-(1-\bar{\sigma}_i)^k}{\sigma_i}\mu_i \quad \forall \quad i \in [0, N-1] \quad (20)$$

with $\bar{\sigma}_i = \frac{\sigma_i}{\sigma_0}$. The equations converge to $\nu_i^\infty = \frac{\mu_i}{\sigma_i}$ for $|1-\bar{\sigma}_i| < 1$. This is always true due to the svd property $\sigma_0 > \sigma_i > 0$.

The convergence speed is determined by $1-\bar{\sigma}_i$. On the other hand, ν_i^∞ is proportional to σ_i^{-1}. Therefore, output components, that require lower input signals are learned faster than components requiring higher input signals. This is a useful feature regarding input saturations or non-minimum phase systems.

8. SIMULATIONS AND CONCLUDING REMARKS

Figures 10 and 11 show simulations of the feedback together with the learning controller. Problems with the saturation of the plant input U_l are avoided by using the above explained learning algorithm. The contact velocity reduces from 0.05 m/sec at $k = 1$ to 0.02 m/sec at $k = 20$. Low contact velocity is associated with low noise and high component reliability. Automotive manufacturers are currently designing and manufacturing camshafts to achieve this requirements in low engine speeds (idle operation). A controller was designed and simulations showed that the EMCV

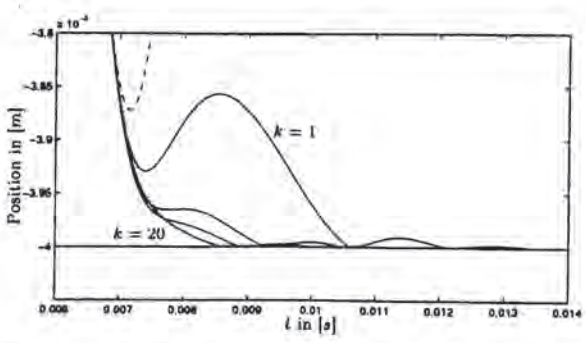

Fig. 10. The position $Y(t)$ tends to the desired position $Y_d(t)$ (dotted) with increasing k. The figure shows $k \in [1, 3, 5, 20]$.

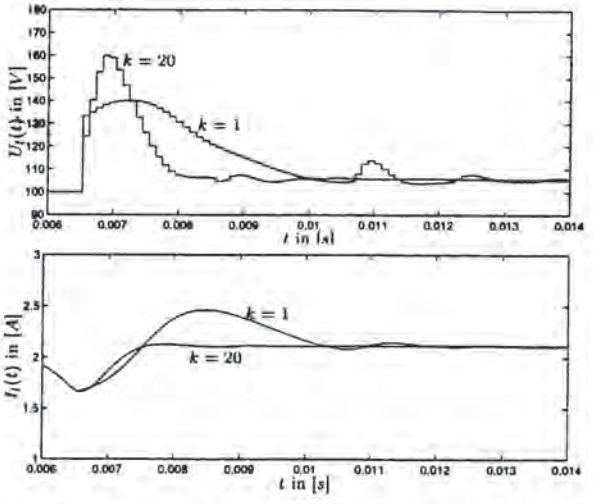

Fig. 11. Upper figure: The voltage $U_l(t)$ remains smaller than the limit of U_l^{max} during the cycles. Lower figure: Current $I_l(t)$ before and after learning.

closed loop system achieves the low contact velocity, and thus, the "soft landing" requirement. The presented controller combines linear feedback and learning feedforward controller.

9. REFERENCES

Arimoto, S., S. Kawamura and F. Miyazaki (1984). Bettering operation of robots by learning. *J. of Robotic Systems* **1**(2), 123–140.

Butzmann, S., J. Melbert and A. Koch (2000). Sensorless control of electromagnetic actuators for variable valve train. *SAE Paper No. 2000-01-1225.*

Wang, Y., A. Stefanopoulou, Mohammad Haghgooie, Ilya Kolmanovsky and Mazen Hammoud (2000). Modeling of an electromechanical valve actuator for a camless engine. *To be presented AVEC 2000.*

Xu, J.-X. and Z. Bien (1998). The frontiers of iterative learning control. In: *Iterative Learning Control* (Z. Bien and J.-X. Xu, Eds.). pp. 9–35. Kluwer Academic Press, Boston.